found with the later metals, being in general much more characteristic of 4d and 5d element chemistry.[28,29]

**Acknowledgment.** The spectrophotometric analyses were greatly assisted by E. S. Peterson, and the magnetic susceptibility measurements, by J. E. Ostenson. We remain indebted to R. A. Jacobson for support of the X-ray diffractometer facilities. This research was supported by the National Science Foundation, Solid State Chemistry, via Grants DMR-8318616 and DMR-8902954, and was carried out in facilities of the Ames Laboratory, DOE.

(28) Corbett, J. D.; McCarley, R. E. In *Crystal Chemistry and Properties of Materials with Quasi-One-Dimensional Structures*; Rouxel, J., Ed.; D. Reidel Publishing Co.: Dordrecht, The Netherlands, 1986; p 179.
(29) Rogel, F.; Zhang, J.; Payne, M. W.; Corbett, J. D. *Adv. Chem. Ser.* **1990**, *226*, 369.

**Supplementary Material Available:** Tables of data collection and refinement information and anisotropic atom displacement parameters for $LiScI_3$ and $Na_{0.5}ScI_3$ (two crystals) (2 pages); listings of $F_o$ and $F_c$ data for the two structures reported (5 pages). Ordering information is given on any current masthead page.

Contribution from the Department of Chemistry, Iowa State University, Ames, Iowa 50011

# Bonding Considerations in Metal Iodide Chain Compounds: $A_xScI_3$ and $MI_3$ (A = Li, Na; M = Zr, Nb)

Peter K. Dorhout and John D. Corbett*

*Received December 4, 1990*

The bonding in four phases containing confacial trigonal-antiprismatic chains $^1_\infty[MI_{6/2}]$ has been examined by extended Hückel methods. The compounds, electron counts, metal periods, and the respective space groups are as follows: $LiScI_3$, $d^1$, equal, $P\bar{6}c2$; $Na_{0.5}ScI_3$, $d^{0.5}$, paired, $P31c$; $ZrI_3$, $d^1$, and $NbI_3$, $d^2$, both paired and $Pmmn$. In $LiScI_3$, a half-filled 1a′ band is generated by $d_{z^2}$ interactions through the shared faces. A Peierls-like pairing distortion is evidently precluded by the stiffness of the lattice; instead, an alternate charge density wave deformation is consistent with the magnetic susceptibility data. The low symmetry and doubled chain period in the unusual $Na_{0.5}ScI_3$ structure combine to open up a gap in the bonding $d_{z^2}$ band at $E_F$ even though higher a′ states are still bonding. The unusual stoichiometry limit is postulated to be thermodynamic in nature. The remainder of this $d_{z^2}$ band is filled in the more normal, metal-paired chains in $ZrI_3$, the predicted semiconduction being in agreement with reported data. Greater pairing displacements in $NbI_3$ increases the $d_{z^2}$ band dispersion. A narrow neighboring a″ band also splits off, and its occupation gives relatively localized $\pi$ bonding in the metal dimers. The compound is also predicted to be a semiconductor. The course of this bonding scheme for later $MI_3$ examples is also considered.

## Introduction

Trihalides of the group III–V transition metals offer some remarkable examples of the various structures attained in response to metal–metal bonding possibilities. The more common $\beta$-$TiX_3$ (or $ZrX_3$) structure has been described as an hcp halogen lattice in which one-third of the octahedral sites are filled by metal atoms so as to generate chains of these atoms perpendicular to the hcp halogen layers.[1-4] This packing generates quasi-infinite chains of confacial octahedra, $^1_\infty[MX_{6/2}]$, an arrangement that would appear to favor pairing of $d^1$ metal atoms to give alternately long and short metal–metal interactions along the chain axis, although such distortions were not recognized for many years.

Recently, detailed studies of the structures of $ZrI_3$[5] and $NbI_3$ (among others)[6] as well as of the closely related $A_xScI_3$ (A = Li, $x = 1$; Na, $x = 0.5$)[7] have revealed that subtle chemical and geometrical changes occur in most of these chain compounds. In the $ZrI_3$ and $NbI_3$ cases, decreases in alternate M–M separations along the chains are accompanied by an orthorhombic distortion of the hcp iodine layers, presumably to better accommodate the intruding M–M bonding. The isostructural $MoI_3$, $MoBr_3$, and $RuBr_3$ have also been so quantified recently.[8] In the $A_xScI_3$ phases, Sc–Sc pairing accompanies the fractional inclusion of sodium into two types of octahedral sites in $Na_{0.5}ScI_3$, whereas full occupation of one type of lithium site in $LiScI_3$ gives a structure in which the confacial iodine octahedra containing $d^1$ atoms show *no* pairing distortions.

These results have prompted us to investigate the impetus and alternatives for bonding in these group III, IV, and V trihalide phases. Extended Hückel treatments of other, somewhat related one-dimensional transition-metal chalcogenides and chlorides have been presented by Whangbo et al.,[9] Bullett,[10] and Shima and Kamimura.[11] However, the chloride studies[10] pertained to $A^IMCl_3$ (hexagonal perovskite) compounds of 3d metals that exhibit only localized metal states, as manifested in their magnetic and insulating properties. On the other hand, properties of the scandium, zirconium, and niobium triiodide phases clearly reflect strong metal–metal interactions, giving rise to several questions that beg for serious consideration: (1) For the $A_xScI_3$ series, why and how does lithium in one set of octahedral sites yield an undistorted $d^1$ chain structure whereas sodium with a fractional occupation of two yields a $d^{0.5}$ system with long–short Sc–Sc interactions? (2) How does the bonding in these two compounds compare with that in the $d^1$ binary $ZrI_3$? (3) How does the bonding in the $MI_3$ host change to accommodate additional electron density on the metal as one goes from group III to group V? Table I lists dimensional data and bonding characteristics for those compounds that are relevant to our inquiry.

## Experimental Section

The atomic positions and unit cell parameters for the title compounds have been described elsewhere.[5-7] Tight-binding, extended Hückel calculations were performed on one-dimensional Brillion zones containing 17 k points along the chain axes, defined in all cases as $z$. This is the

(1) Wells, A. F. *Structural Inorganic Chemistry*, 5th ed.; Oxford: Oxford, U.K., 1984; p 419.
(2) Holze, E. Dissertation, Westfälische Wilhelms Universität, Münster, FRG, 1956.
(3) Dahl, L. F.; Chiang, T.-I.; Seabaugh, P. W.; Larsen, E. M. *Inorg. Chem.* **1964**, *3*, 1236.
(4) Natta, G.; Corrandia, P.; Bassi, I. E.; Porri, L. *Atti. Accad. Naz. Lincei, Cl. Sci. Fis. Mat. Nat., Rend.* **1958**, *24*, 121.
(5) Lachgar, A.; Dudis, D. S.; Corbett, J. D. *Inorg. Chem.* **1990**, *29*, 2242.
(6) Krebs, B.; Rüssman, U. Private communication, 1986.
(7) Lachgar, A.; Dudis, D. S.; Dorhout, P. K.; Corbett, J. D. *Inorg. Chem.*, preceding paper in this issue.
(8) Hillebrecht, H. Doctoral Dissertation, Albert-Ludwigs Universität, Freiberg, FRG. Thiele, G. Private communication, 1991.
(9) Whangbo, M.-H.; Foshee, M. J.; Hoffmann, R. *Inorg. Chem.* **1980**, *19*, 1723.
(10) Bullett, D. W. In *Theoretical Aspects of Band Structures and Electronic Properties of One-Dimensional Solids*; Kamimura, H., Ed.; Reidel: Dordrecht, The Netherlands, 1986; p 27.
(11) Shima, N.; Kamimura, H. In ref 10, p 231.

0020-1669/91/1330-3326$02.50/0 

**Table I.** Lattice Dimensions (Å), Space Groups, and Metal–Metal Characteristics in Confacial Chain Triiodides[a]

| | *a* | *b* | *c* | space group | M–M spacing | short d(M–M), Å | bond order |
|---|---|---|---|---|---|---|---|
| $LiScI_3$ | 7.286 (9) | | 6.768 (2) | $P\bar{6}c2$ | equal | 3.38 | 0.17 × 2 |
| $Na_{0.5}ScI_3$ | 7.479 (1) | | 13.699 (3) | $P31c$ | paired | 3.27 | 0.26 + 0.08[b] |
| $ZrI_3$ | 12.594 (6) | 6.679 (2) | 7.292 (2) | *Pmmn* | paired | 3.17 | 0.38 + 0.10[b] |
| $NbI_3$ | 12.140 (5) | 6.353 (4) | 7.009 (5) | *Pmmn* | paired | 2.71 | 1.00 + 0.03[b] |
| $MoI_3$ | 12.322 (4) | 6.420 (4) | 7.115 (2) | *Pmmn* | paired | 2.86 | 0.40 + 0.03[b] |
| $OsI_3$ | 12.12 (2) | 6.277 (7) | 7.012 (9) | *Pmmn* | paired | 2.90 | 0.24 |

[a] These data pertain to room temperature structures[5,7,8] except for $NbI_3$, which was studied at 140 K.[6] [b] Pauling bond order for the long M–M separation.

**Table II.** Parameters Used in Extended Hückel Calculations

| atom | orbital | $H_{ii}$, eV | $\zeta_1$[a] | $\zeta_2$[a] | $C_1$ | $C_2$ |
|---|---|---|---|---|---|---|
| Sc[b] | 4s | −8.87 | 1.30 | | | |
| | 4p | −2.75 | 1.30 | | | |
| | 3d | −8.51 | 4.35 | 1.70 | 0.4228 | 0.7276 |
| Zr[c] | 5s | −7.78 | 1.82 | | | |
| | 5p | −4.96 | 1.78 | | | |
| | 4d | −8.65 | 3.84 | 1.51 | 0.6213 | 0.5798 |
| Nb[d] | 5s | −7.92 | 1.89 | | | |
| | 5p | −4.15 | 1.85 | | | |
| | 4d | −8.26 | 4.08 | 1.64 | 0.6401 | 0.5516 |
| I[c] | 5s | −20.84 | 2.68 | | | |
| | 5p | −11.21 | 2.32 | | | |

[a] Exponent in the double-$\zeta$ function for d orbitals. [b] References 12a and 13. [c] Reference 14. [d] References 12b and 13.

crystallographic *c* axis in the scandium compounds and the *b* axis in $ZrI_3$ and $NbI_3$. The zone boundary for the hexagonal lattices of the scandium compounds is, as before, denoted as X (although the convention is A), while this point is Y in the orthorhombic cells of the binary triiodides. Interactions between the iodine-sheathed chains involve only shared Li and Na atoms or van der Waals forces ($ZrI_3$, $NbI_3$). Earlier studies have shown that such structures may be treated as one-dimensional, neglecting interchain interactions.[9] The unit $^1_\infty[Sc_2I_6]$ pertains to $LiScI_3$ while $^1_\infty[M_4I_{12}]$ applies to M = Sc (Na), Zr, and Nb where there is metal pairing.

The atom parameters $H_{ii}$, *C*, and $\zeta$ utilized are listed in Table II. The orbital parameters for Sc and Nb were derived from self-consistent-field calculations cited by Richardson et al. and by Basch and Gray.[12] Energy parameters for the same two elements were derived from charge-iterative calculations reported by Hoffman.[13] Those for Zr and I were obtained from charge-iterative calculations of $Zr_6I_{18}Fe$.[14] The alkali-metal cations were not included in the calculations since their electronic effects cannot be accurately described with this method. Coulombic contributions to stability have been neglected as well. We have therefore allowed for only the consequences of electron donation from the higher lying and poorly admixed alkali-metal bands on the valence band populations. The symmetries of the alkali-metal distributions do reflect important consequences of symmetry on the band structures, however. A smoothing parameter of 0.05 eV was applied to the DOS and COOP plots.

## Structures

A brief synopsis of the structures of all of these compounds is in order so that later discussions on bonding may be understood.

**$LiScI_3$.** The hexagonally close-packed iodine layers are separated by equally spaced scandium atoms ordered in chains, producing regular confacial $ScI_{6/2}$ trigonal antiprisms along *c*,[7] that is, the idealized form of the $\beta$-$TiCl_3$ structure type ($P6_3/mcm$).[2-4] Further reduction of symmetry to $P\bar{6}c2$ results from the introduction of the lithium atoms into one of the other two chains of octahedral sites. A portion of the resulting $LiScI_3$ chains is shown in Figure 1A. Parallel chains are held together by the lithium ions with their six antiprismatic iodine neighbors (two each from three chains).

**$Na_{0.5}ScI_3$.** The basic building blocks are again the $ScI_{6/2}$ confacial octahedra, but reduction of symmetry ($P\bar{6}c2 \rightarrow P31c$)

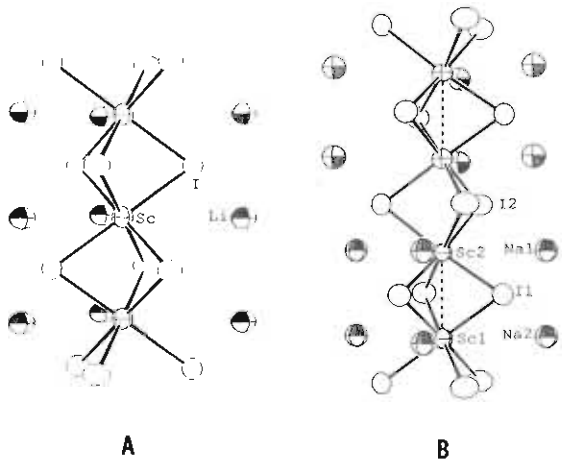


A B

**Figure 1.** [110] views of a portion of one chain in (A) $LiScI_3$ and (B) $Na_{0.5}ScI_3$. These span two cell lengths and one cell length along $\vec{c}$, respectively.

and a doubling of the unit cell along *c* is accompanied by ~50% sodium occupancy of two independent octahedral sites. These pair to produce trigonal prisms of sodium atoms about the short Sc–Sc separation, the orientation of which alternates by 60° along the chain.[7] The symmetry at the metal is lowered from $C_{3v}$ to $C_3$. There are only subtle changes in the hcp iodine layers. A view of a portion of the $Na_{0.5}ScI_3$ chain is shown in Figure 1B. The dashed lines between Sc1 and Sc2 emphasize the short interactions, 3.278 (5) Å vs 3.572 (5) Å for the long separation and 3.384 (1) Å for all Sc–Sc in the Li compound. Additionally, the I1 and I2 triangles within the close-packed iodine layers that circumscribe the Sc chain do not expand or contract in size, respectively, in constrast to the behavior of the iodine atoms in $ZrI_3$ and $NbI_3$ (below). Rather, the paired scandium atoms lie closer to the invervening I1 atoms, creating a distorted octahedral arrangement of iodine atoms around Sc (see **1**).

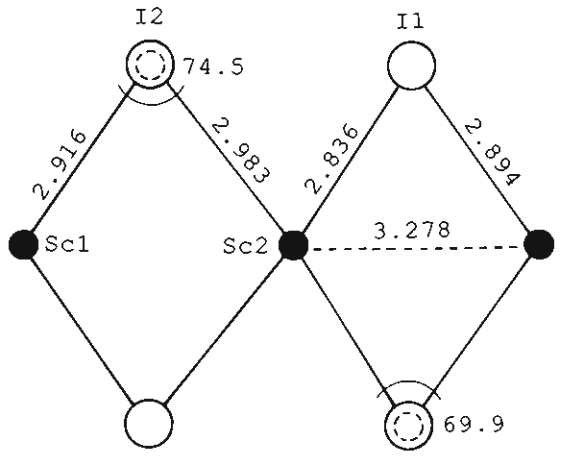


**1**

**$ZrI_3$.** The $d^1$ and $d^2$ iodides $ZrI_3$ and $NbI_3$ also exhibit reduced symmetry, *Pmmn*. Figure 2 illustrates the confacial $ZrI_{6/2}$ octahedra in $ZrI_3$,[5] which are distorted through pair formation

(12) (a) Richardson, J. W.; Nieuwpoort, W. C.; Powell, R. R.; Edgelol, W. F. *J. Chem. Phys.* **1962**, *36*, 1057. (b) Basch, H.; Gray, H. B. *Theor. Chim. Acta* **1966**, *4*, 367.
(13) Hoffmann, R. Unpublished program package.
(14) Hughbanks, T.; Corbett, J. D. *Inorg. Chem.* **1989**, *28*, 631.

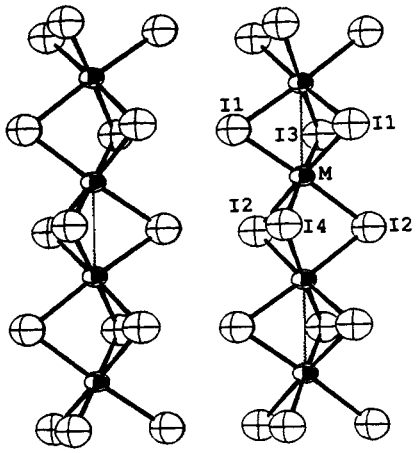


**Figure 2.** [101] view of a pair of neighboring chains in $MI_3$ (M = Zr, Nb), showing two of the quasi-infinite chains that run parallel to *b*. Alternating short M–M distances are dashed.

accompanied by alternate expansion and contraction of the iodine shared faces, **2**. Expanded iodine triangles (I1–I3 = 4.148 Å,

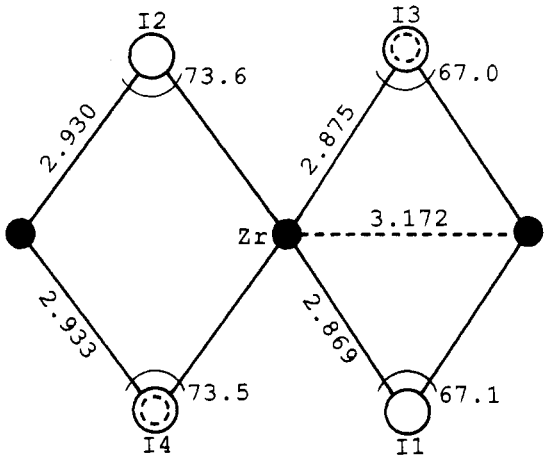


**2**

I1–I1 = 4.130 Å) circumscribe the short Zr–Zr bond, while contracted iodine triangles (I2–I4 = 4.068 Å, I2–I2 = 4.062 Å) surround the long Zr–Zr interaction. Packing of these distorted chains results in loss of the 3-fold axis along the metal chain and reduction of the point symmetry at Zr from $C_{3v}$ to $C_s$, the long and short bonds alternating within [101], Figure 2.

**$NbI_3$.** The structure of the isostructural $d^2$ $NbI_3$ has been determined only at 140 K,[6] a temperature difference that reduces $d$(Zr–Zr) in $ZrI_3$ by about 0.26 Å.[5,6] The short Nb–Nb bond, 2.708 Å, is close to the Pauling single-bond length for the metal.[15] The Nb–I distances are, as expected, significantly less than those in $ZrI_3$, and this decreases the intrachain I1–I3 and I2–I4 iodine distances by 0.21 and 0.15 Å, respectively. Although some of this is the result of temperature differences, the greater part of the effect of shorter Nb–Nb separation on the I···I distances is compensated for by shorter Nb–I distances. Thus, the greater pairing distortion within the chain is accompanied by a decrease in I···I chain diameters and less comparative "breathing" of the iodine triangles in the shared faces.

## Bonding

It is important to note the properties of the metal d orbitals in these pseudooctahedral environments. The usual octahedral coordinate system is not appropriate for chains of face-sharing octahedra since the *z* axis is defined as the chain axis and is not directed toward an apex as is traditional. Following Whangbo et al.,[9] the natural combinations of metal d orbitals that point between the iodine atoms are $d_{z^2}$ and normalized combinations

(15) Corbett, J. D. *J. Solid State Chem.* **1981**, *37*, 335.

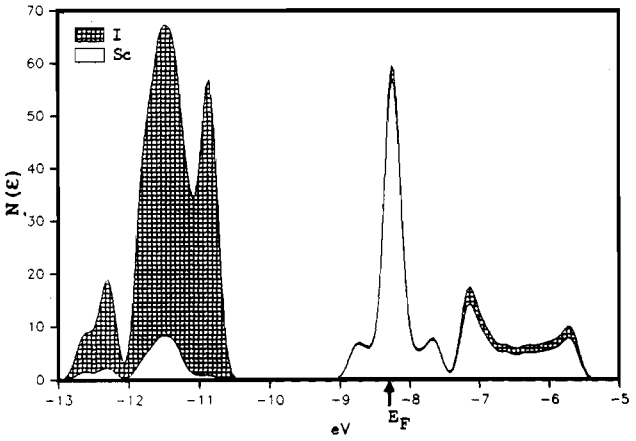


**Figure 3.** DOS plot for $LiScI_3$ showing the distinctive Sc–I bonding and nonbonding I 5p pairs (−13.0 to −10.5 eV) and the Sc d-orbital contributions (−9.0 to −5.5 eV). The I and Sc contributions are projected out.

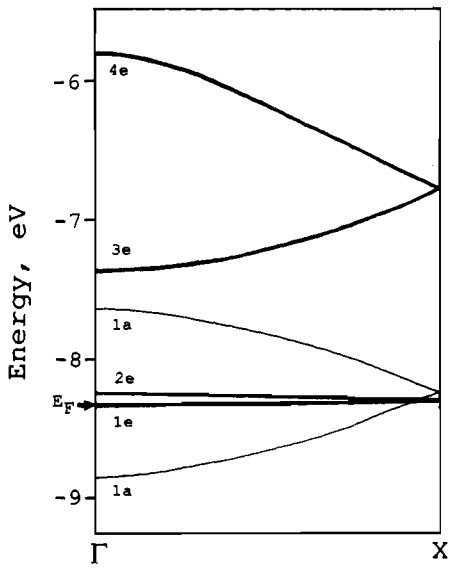


**Figure 4.** Sc d-orbital band structure diagram for $LiScI_3$ between Γ and X. The darker bands are doubly degenerate (1e and 2e).

of $d_{xy} - d_{xz}$ and $d_{x^2-y^2} - d_{yz}$, i.e., a $t_{2g}$-like set, while the orbitals that are directed toward the iodine atoms, $d_{xy} + d_{xz}$ and $d_{x^2-y^2} + d_{yz}$, belong to an $e_g$-like set. In later representations, we will use the a.o.'s that make up these and not the combinations themselves.

**$LiScI_3$.** The total densities-of-states (DOS) plot in Figure 3 also contains the Sc and I contributions to the total DOS. The structures of the bands within the Brillion zone along the line between Γ and X for the $^1_\infty[ScI_{6/2}]_2$ chain are shown in Figure 4, with symmetry assignments according to the $C_{3v}$ point symmetry at the metal. The classic two-above-three ($e_g$- and $t_{2g}$-like) d-based bands on scandium above −9.2 eV are a product of the nominal octahedral environment of iodines around scandium. The most important feature is that the metal $d_{z^2}$ band (1a) within the "$t_{2g}$" set is broadened by Sc–Sc interactions through the shared faces of the iodine octahedra. The composition of the four low-lying 1a and 1e bands in this set at the zone center, Γ, and a pair of Bloch-related functions at X that are necessary to see the correct form are schematically illustrated in **3**.

The dominant interactions that define the two 1e bands involve iodine p orbitals in the valence band around −11 to −12 eV. The in-phase metal–metal combinations (antibonding to iodine) then lie in the upper regions of this group while those in the lower e band are out of phase for Sc–Sc bonding. Population of metal–metal bonding $\pi$ and $\delta$ states will later be seen to alter the flavor of these bands.

One important feature of Figure 4 and **3** is that a small portion of the narrow 1e band, which is nonbonding at X, is calculated

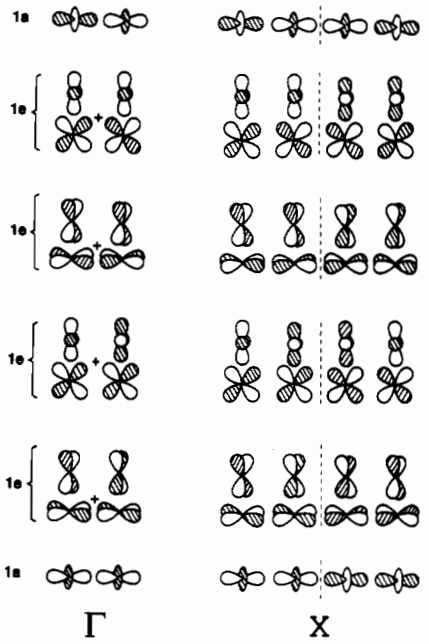


3

to start filling near Γ before the 1a band is half-full. However, the magnetic character of $LiScI_3$[7] as well as of all other compounds we are considering here makes it clear that M–M interactions are dominant and that we are not dealing with localized M states in the magnetic, insulating materials commonly found for $A^IMX_3$ or $MX_3$ with M = Ti, V, .... As far as the present result, it is well-known that the application of Bloch functions in one-electron calculations does a poor job of describing electrons in narrow bands, these tending toward, or being better described by, localized states on, in this case, scandium, rather than well-delocalized electrons in a broader d band. This arises because intrasite electron–electron repulsions become important in the energetics. Their effects will certainly be to raise the two e bands and to place $E_F$ at X in the 1a band. We have not shown COOP plots for $LiScI_3$ because of the misleading character that this e band misplacement gives. Their character will be evident from later considerations of other compounds.

We are now left with a classic, half-filled band that, strangely enough, is not undergoing the expected Peierls distortion and dimerization. We note that only e representations are allowed at X in this space group ($D_{3h}^2$),[16] so splitting of the band is not possible. This and the character of the susceptibility lead us to conclude that an alternate process for lowering the energy of the half-filled 1a band, formation of a charge density wave (CDW), has probably taken place in $LiScI_3$.[7]

The relatively strong lithium interactions with their local iodine environments, both covalent and Coulombic, must provide a stiffening of the lattice that precludes the alternate pairing (or other commensurate) distortions of the chains at room temperature as occur in the sodium analogue and in $ZrI_3$.

**$Na_{0.5}ScI_3$.** The structural changes that accompany the formation of this compound are in the character of a Peierls distortion of the Sc–Sc chain. However, the nature of this is quite different from that of $ZrI_3$ in that the $c$ axis is doubled. The surprising $d^{0.5}$ metal configuration is intimately related to the details of the structure (Figure 1B) and its bonding.

The DOS curve with Sc and I contributions to the total projected out is shown in Figure 5. The differences between the $LiScI_3$ and $Na_{0.5}ScI_3$ results are subtle. The band folding that reflects the doubling of the unit cell along $\vec{c}$ is evident in the band structures in Figure 6, where the Fermi energies are marked for $Na_xScI_3$ compositions of $x = 0.5$ (known) and 1.0 (hypothetical). The metal dimerization opens a gap of about 0.3 eV between the

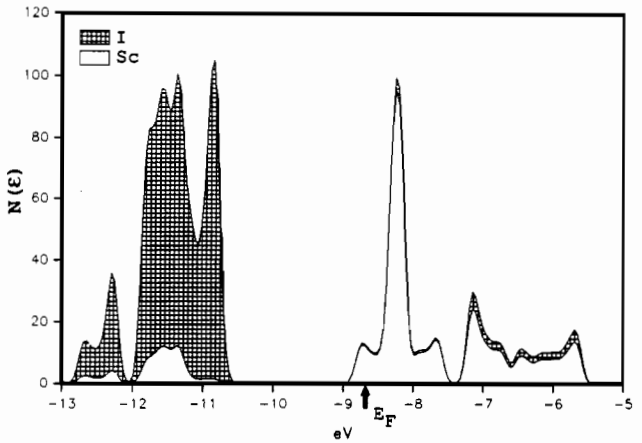


**Figure 5.** DOS plot for $Na_{0.5}ScI_3$ showing the Sc–I bonding and I nonbonding region (−13.0 to −10.5 eV) and the Sc d-band region (−9.0 to −5.5 eV).

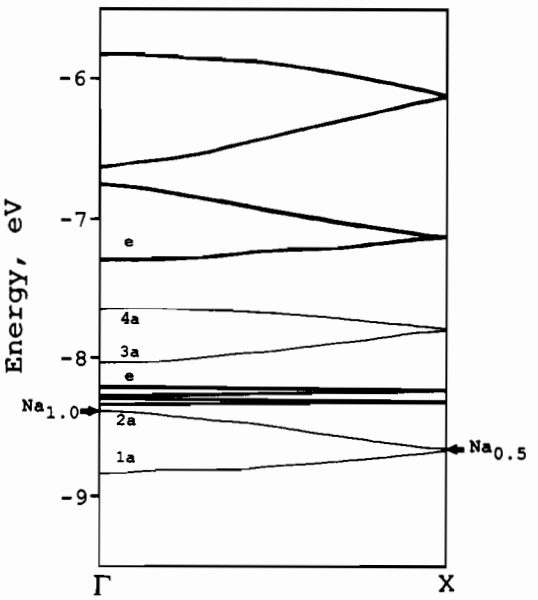


**Figure 6.** Band structure of $Na_xScI_3$ between Γ and X. The darker bands are doubly degenerate. The calculated Fermi levels for $x = 0.5$ and 1.0 are marked.

bonding 1a, 2a bands and the more antibonding 3a, 4a bands generated from metal $d_{z^2}$, with a concomitant lowering of the energy of the former pair below the four narrow e bands. The last are again doubtlessly placed too low in the absence of electron repulsion considerations. The several narrow energy gaps in this region are quite obscured in the smoothing applied in Figure 5. Of particular importance is the fact that X is not a special point for this noncentrosymmetric cell ($C_{3v}^4$), and the two 1a, 2a bands do not become degenerate there but retain a gap. In other words, the unusual composition $Na_{0.5}ScI_3$ has a filled Sc–Sc bonding band, and an electronic instability is not to be expected. Half-occupancy of cation sites in a $LiScI_3$-like arrangement but with dimerization would not do the same.

The crystal orbital overlap population (COOP) curves shown in Figure 7 and the orbital representations for the metal $\sigma$ bands given in **4** illustrate something of the character of the bonding

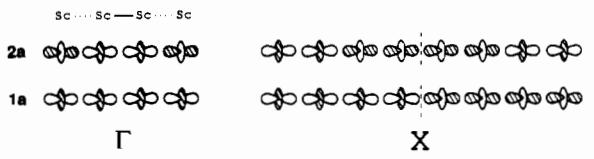


4

in the bands around $E_F$. The bonding at Fermi may be described

(16) Kovalev, O. V. *Irreducible Representations of the Space Groups*; Gordon and Breach: New York, 1965.

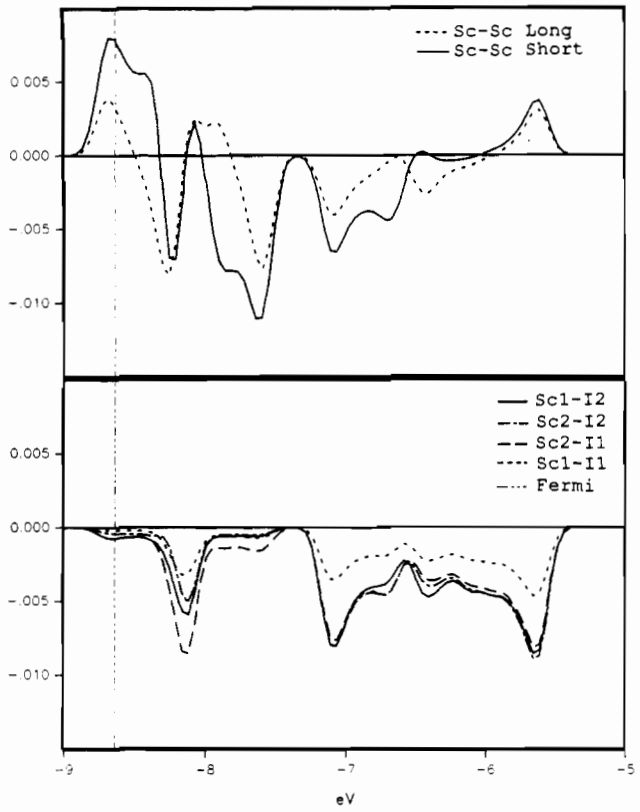


**Figure 7.** COOP curves for Sc–Sc and Sc–I pairwise interactions in $Na_{0.5}ScI_3$ as a function of energy (eV): (+) bonding; (−) antibonding.

as a combination of Sc–Sc bonding plus small Sc–I interactions that are roughly nonbonding. In fact, the shorter Sc–Sc separations remain bonding up to a composition near $Na_{1.0}ScI_3$ ($E_F$ = −8.4 eV) while the long Sc···Sc interactions show smaller but still largely bonding (in phase) contributions only up to $Na_{0.5}ScI_3$ and become appreciably antibonding beyond that point (Figure 7). Figure 8 shows the overlap populations as a function of electron count (indirectly, the number of sodium atoms in the unit cell). A maximum overlap for the long Sc–Sc separation (bond order = 0.08) occurs at the observed 98 electrons per unit cell, whereas that for the short Sc–Sc distance (bond order = 0.27) increases steadily with increasing electron count. (The e bands would affect the picture only above 100 electrons per cell.) Increasing the electron count beyond 98 populates more antibonding Sc–I states, but these changes are small in comparison. According to Figures 6–8, an increased reduction beyond the observed $Na_{0.5}ScI_3$ would clearly result in increased bonding and presumably increased pairing distortion (but an open shell until $Na_{1.0}ScI_3$). The reason for the unusual stoichiometry is apparently not to be found in these features.

The present $Na_{0.5}ScI_3$ provides a nice example of the need to consider extended, delocalized states, even in such a seemingly simple case. A naive localized view of the bonding in $Na_{0.5}ScI_3$ would suggest an unusual mode with half-bonds between scandium pairs, whatever that would imply magnetically, and would provide no interpretation of the stoichiometry. But the basic reason why $NaScI_3$ did not form instead of $Na_{0.5}ScI_3$ is less obvious as this should clearly give stronger dimer bonding. One plausible explanation is thermodynamic in character, that scandium metal is not a strong enough reducing agent to afford scandium(II) in the ternary system and the present result is a novel alternative to no reduction at all. In addition, the known and incompletely reduced $Sc_{0.93}I_2$[17] (=$ScI_{2.15}$) (plus NaI) would constitute an alternative product were further reduction to take place.

**$ZrI_3$.** The structural deviations of $ZrI_3$ from the idealized $\beta$-$TiCl_3$-like structure have been discussed earlier.[5] As for

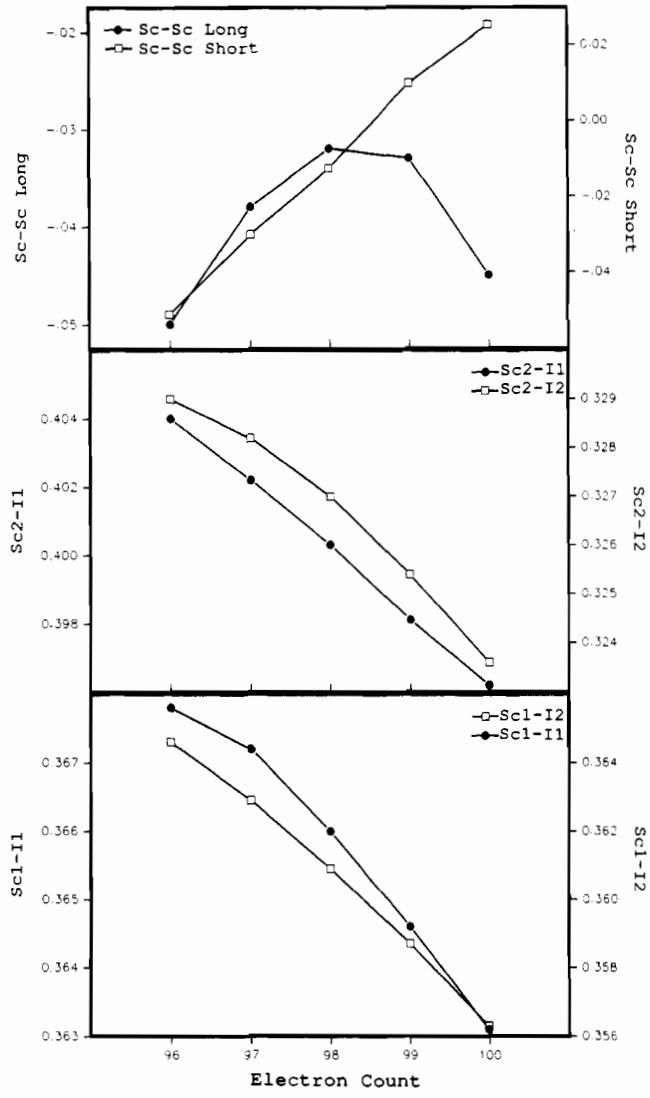


**Figure 8.** Sc–Sc and Sc–I overlap populations for $Na_{0.5}ScI_3$ as a function of electron count.

$Na_{0.5}ScI_3$, these consist of a Peierls-like distortion of the metal chain but now with the nominal formation of more conventional two-electron bonds in dimers. The problem is also different because of the weaker interchain interactions in the absence of alkali-metal cations, a loss of 3-fold symmetry in the chains, an alternating expansion and contraction of the shared triangular iodine faces along the chain, a primitive orthorhombic lattice, and a lowering of the point symmetry at the metal to $C_s$. The DOS and band structure diagrams accordingly display some major differences from those seen earlier.

The DOS data, Figure 9, show the expected valence band plus an apparent metal-dominated "conduction" band that has broadened considerably with respect to the scandium examples owing to the stronger metal–metal interactions. As shown in the band structure diagram in Figure 10, a number of gaps are obscured by the smoothing applied to Figure 9, the most important of which is that at $E_F$ (−7.9 eV), the top of the $d_{z^2}$ band. The remaining d bands are nominally antibonding for Zr–Zr (see **4**) and for Zr–I and are calculated to lie in a narrow region above Fermi. These are a″ and no longer degenerate except at Y as a result of the lower symmetry; they are again doubtlessly placed too low in energy. The $d_{z^2}$ bands are in contrast broad, and a notable gap of 0.8 eV is calculated between the upper and lower a′ bands.

The COOP curves, Figure 11, illustrate that the short Zr–Zr separations (bond order = 0.38) remain bonding up to $E_F$ whereas an antibonding character enters into the long Zr–Zr interaction (bond order = 0.10) in the upper half of a′. This aspect closely

(17) McCollum, B. C.; Dudis, D. S.; Lachgar, A.; Corbett, J. D. *Inorg. Chem.* **1990**, *29*, 2030.

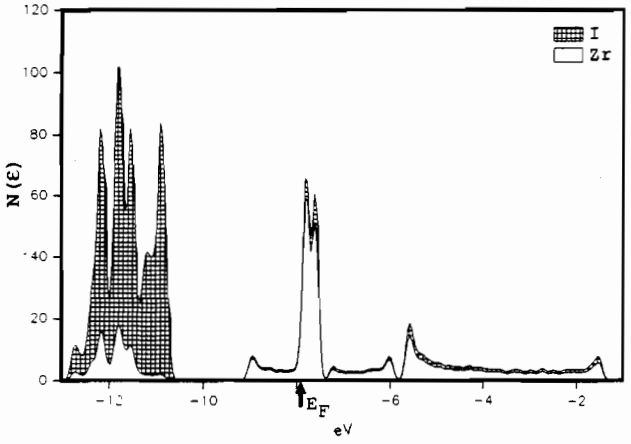


**Figure 9.** DOS plot for $ZrI_3$ showing the Zr–I bonding and nonbonding I 5p region (−13.0 to −10.5 eV) and the broadened Zr d bands above −9.0 eV.

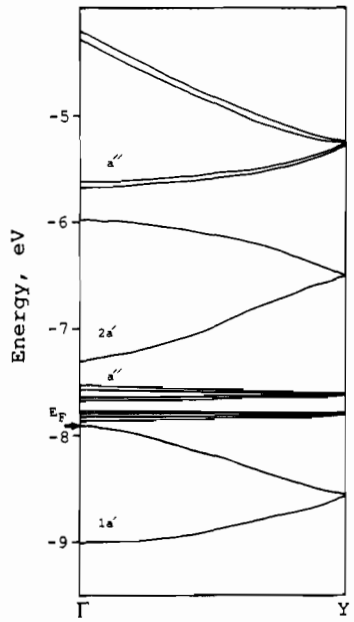


**Figure 10.** Band structures for $ZrI_3$ between Γ and Y. Note the gap at $E_F$.

parallels the result for $Na_xScI_3$, Figure 7. Even shorter and stronger Zr–Zr bands are presumably precluded by iodine matrix effects.[15] It is informative to note the low charges that may be approximated (in the Mulliken sense) for Zr (∼+0.25) and I (≃−0.04 to −0.13) when self-consistent values for $H_{ii}$ (based on $Zr_6I_{18}Fe$) are used. Predominantly covalent bonding is indicated.

The obvious gap at $E_F$, Figure 10, is consistent with the reported low semiconduction of $ZrI_3$, $\sim 2 \times 10^{-4}\ \Omega^{-1}\ cm^{-1}$ at room temperature.[18] Magnetic properties seem to be more problematical because of apparently substantial effects of impurities, but some paramagnetism is suggested.[7,19] Nonstoichiometry on the oxidized side up to ca. $Zr_{0.88}I_3$[20] may be a complicating feature; this might be expected to lead to both vacancies and $Zr^{IV}$ on normal metal sites.

**$NbI_3$.** This phase is isostructural with $ZrI_3$,[6] but it has twice the d-electron complement and appreciably more chain asymmetry because of greater metal pairing displacements. The smaller metal atom has also changed some proportions in the chains, as noted earlier.

The DOS curves of $NbI_3$, Figure 12, are similar to those found for $ZrI_3$ except for a greater dispersion of the 1a′ and 2a′ bands

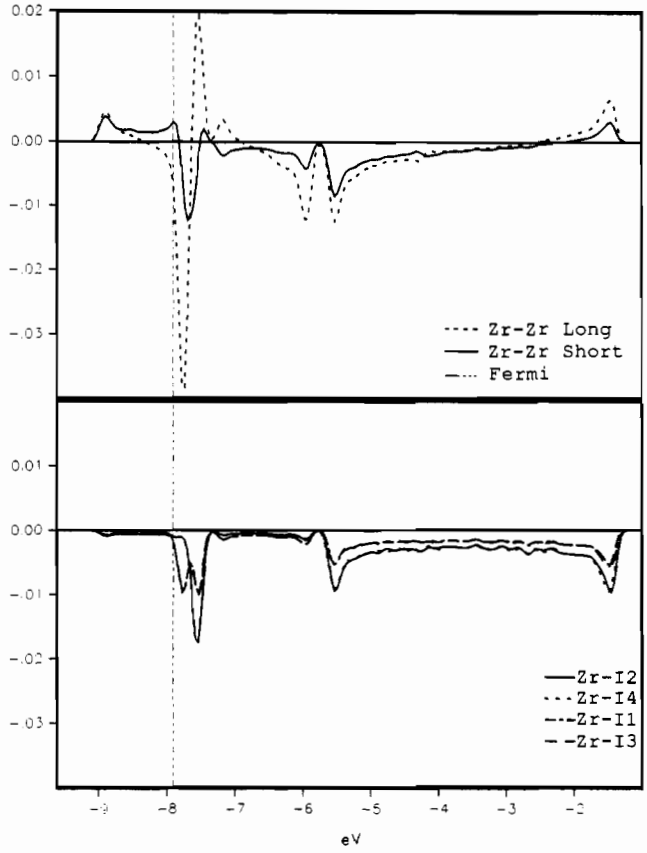


**Figure 11.** COOP curves for $ZrI_3$ near and above the Fermi level. Bonding (+) and antibonding (−) contributions are shown for various Zr–Zr and Zr–I pairs.

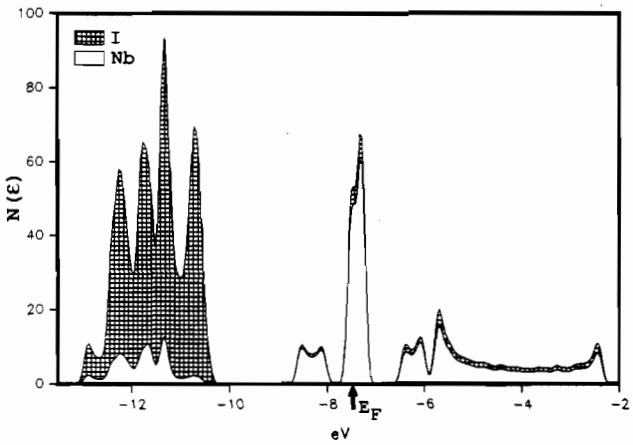


**Figure 12.** DOS plot for $NbI_3$, with atom contributions projected out.

that result from bonding interactions, Figure 13. The Fermi level now lies in a narrow gap above the first of a group of four narrow a″ bands that become degenerate only at Y. Their precise location and dispersion is again problematical, of course. As illustrated in **5** (at Γ only), the filled a″ band is now π and δ Nb–Nb bonding in character for the short bonds. These band compositions and the COOP curves, Figure 14, show that the long Nb···Nb separations are basically antibonding above −8.3 eV, that is, for the upper half of the 1a′ band and all of the occupied a″ band. Thus, the additional electrons are in a sense localized in the short double bonds, appropriate to the narrowness of these bands. The contrasting bond order of 1.0 for the short Nb–Nb separation must reflect the significant resistance of the iodine matrix to the pairing distortion.

It is interesting to note the change in orbital character of the 1a″ bands between $ZrI_3$ and $NbI_3$. In $ZrI_3$, the a″ bands just above Fermi were strongly antibonding in character (Figure 11), whereas

(18) Clemmer, R. G. Ph.D. Thesis, University of Wisconsin, 1977.
(19) Feldman, C. D. Ph.D. Thesis, University of Wisconsin, 1979.
(20) Daake, R. L.; Corbett, J. D. *Inorg. Chem.* **1978**, *17*, 1192.

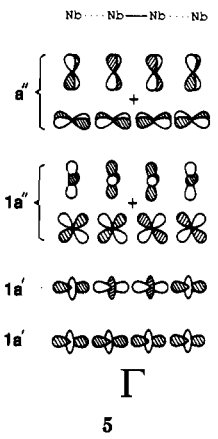


5

in $NbI_3$ these bands have become bonding for the Nb–Nb short interaction. These observations are in accord with the general tendency of antibonding orbitals in such a narrow band to "float" to the top of the band as the metal–metal interactions become more important[9] (the obverse is true for compounds with little M–M interaction; see **3**). As a consequence, the long Nb···Nb interactions have become dramatically antibonding. This of course reflects a common characteristic of stable compounds, a sharp break in bonding character at or near $E_F$, and it assures us that the calculational results are plausible and reflect likely bonding circumstances. The bonding distances are the principal variables in the input.

There are very few observations on $NbI_3$ properties that might correlate with the predictions that can be made on the basis of Figure 13, the most credible of which is that the phase should be a semiconductor. The existence of the gap within this type of compound is reasonable, but its size is unknown. A room-temperature (Guoy) observation on several grams of $NbI_3$ found it to be diamagnetic,[21] although a very weak paramagnetism possibly could have been obscured by the diamagnetism of the glass container. Paired metals in a chain-type structure for $NbX_3$ is unique to the iodide, the chloride and bromide evidently forming $NbX_3$ compounds with dimers in layer structures based on $CdI_2$.[22] All three form trimers in layered $Nb_3X_8$ structures, too.[22,23] In both of these cases, the metal–metal bonding takes place through shared edges of the $NbX_6$ units, while the shared-face arrangement in $NbI_3$ provides obvious advantages for Nb–Nb bonding in the presence of the larger iodide. Niobium triiodide also seems to be somewhat metastable on the basis of two independent studies.[21,24]

Recent structural findings on the isostructural $MoI_3$ and $OsI_3$[8] are also germane to our calculations. The M–M pairing distances in these triiodides are longer than that in $NbI_3$ (at 140 K), corresponding to smaller Pauling bond orders (Mo–Mo, 0.4; Os–Os, 0.24) for metals that have increasingly smaller d orbitals (Table I). These reflect substantially diminished $\sigma$, $\pi$, and $\delta$ interactions as well as the effects of electron–electron repulsion in the increasingly narrow and more nearly localized a″ bands. In fact, the adjoining $RhI_3$ and $IrI_3$ are not known in this arrangement, presumably because this would require filling the antibonding 2a′ band. They crystallize instead in space group $C2/m$ in a layered $\alpha$-$RuCl_3$ arrangement with an M–M separation of ~3.91 Å in the former.[25]

## Conclusions

With regard to the questions posed in the Introduction, the following points may be made.

(1) The contrast between the undistorted $LiScI_3$ and the metal-paired but substoichiometric $Na_{0.5}ScI_3$ illustrates some of the variety of responses available to systems that "should" undergo a Peierls distortion. The stiffness of the lithium-bound lattice evidently precludes the classic pairing distortion; instead, a charge density wave appears to lower the energy of the system. The $d^{0.5}$ sodium system, with a lower reduction limit apparently required thermodynamically, occurs in such a low-symmetry superstructure that the Sc–Sc bonding band is split and pairing with "half-bonds" occurs. Metal–metal bonding states are incompletely occupied. Continuing studies on related systems are expected to provide further clarification and refinement of these ideas and the range

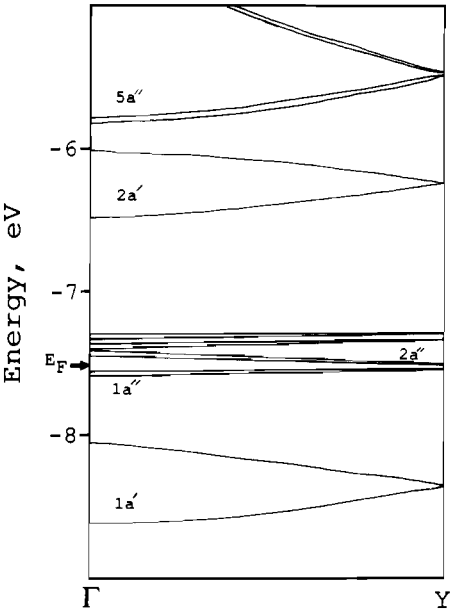


**Figure 13.** Band structures for $NbI_3$ between Γ and Y. Note the gap at $E_F$.

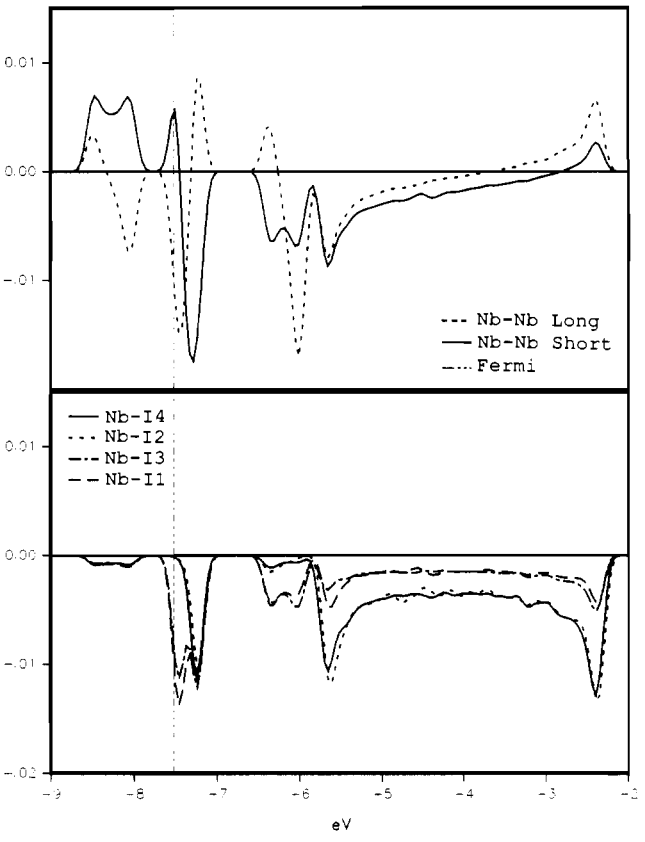


**Figure 14.** COOP curves for $NbI_3$ in the region of the Fermi level. Bonding (+) and antibonding (−) contributions for various Nb–Nb and Nb–I pairs are plotted vs energy.

(21) Seabaugh, P. W.; Corbett, J. D. *Inorg. Chem.* **1965**, *4*, 176.
(22) Schäfer, H.; Schnering, H.-G. *Angew. Chem.* **1964**, *76*, 833 and references therein.
(23) Simon, A.; von Schnering, H.-G. *J. Less-Common Met.* **1966**, *11*, 31.
(24) Simon, A. Private communication, 1990. Simon, A. Doctoral Dissertation, Münster, FRG, 1966.
(25) Broderson, K.; Thiele, G.; Recke, I. *J. Less-Common Met.* **1968**, *14*, 151.

of possibilities. Direct resistivity measurements on these two phases will not be easy because of their extreme sensitivity to moisture, air, cements, etc.

(2) The structure of the $d^1$ binary $ZrI_3$ is a continuation of the metal-metal bonding seen in $Na_{0.5}ScI_3$, achieving complete filling of the $d_{z^2}$ band and paired metal atoms. Increased metal pairing and broadening of the M-M $\sigma$ bands are evident.

(3) The low-lying bands that are antibonding for M-M $\pi$ and $\delta$ interactions in $LiScI_3$ and $ZrI_3$ change with increased metal pairing to afford relatively localized $\pi$ and $\delta$ bonding in $NbI_3$. A further increase in the number of d electrons combined with substantial iodine matrix effects and shrinking orbitals should lessen M-M bonding markedly for isostructural $MI_3$ compounds of later elements.

**Acknowledgment**. We are indebted to A. Lachgar for preliminary calculations, to A. Guloy and G. J. Miller for valuable advice on several points, and to B. Krebs and G. Thiele for sharing their unpublished structural data. This research was supported by the National Science Foundation, Solid State Chemistry, via Grant DMR-8902954 and was carried out in facilities of the Ames Laboratory, DOE.

---

Contribution from the Department of Chemistry, University of Victoria, P.O. Box 3055, Victoria, British Columbia, Canada V8W 3P6

# (Phosphinoalkyl)silyl Complexes. 10.[1] Formation of Chelated Bis[(diphenylphosphinoethyl)diorganosilyl]platinum(II) Complexes. Precoordination through Phosphorus, Intermediacy of a Platinum(IV) Disilyl, and Diastereoisomerism at Planar Platinum(II) in "Chelate-Assisted" Hydrosilylation

Stephen L. Grundy, Rupert D. Holmes-Smith, Stephen R. Stobart,* and Mark A. Williams

*Received December 13, 1990*

Addition of the silane $PPh_2CH_2CH_2SiMe_2H$ (chelH, **1a**) to $Pt(COD)_2$ (COD = cycloocta-1,5-diene) affords in high yield the cis-bis chelate $Pt(chel)_2$ (**2**); formation of the same product from Pt(COD)(X)Y (X = Y = Me; X = Me, Y = Cl) has been shown by NMR spectroscopy ($^1H$, $^{31}P$, $^{195}Pt$) to proceed via prior coordination of chelH through P to afford $Pt(chelH)_2(X)(Y)$ (cis and trans isomers) and through intermediacy of $PtH(chel)_2Cl$ (**22**) in which P trans to Si at Pt(IV) leads to an exceptionally low $^2J(Pt-P)$ = 1084 Hz. Cleavage of Pt-Si bonds in **2** by HCl can be controlled to give the monochelate species Pt(chel)(chelH)Cl (**7**), from which chelH is displaced by $PMe_2Ph$, or *trans*-$PtH(PPh_2CH_2CH_2SiMe_2Cl)_2Cl$ (**9**). Products related to **9** result from Pt-Si bond cleavage by $I_2$ or MeI. Using the analogue $PPh_2CH_2CH_2SiMe(Ph)H$ (**1c**) of **1a**, the analogue Pt-$[PPh_2CH_2CH_2SiMe(Ph)]_2$ (**4**) of **2** is obtained as a mixture of meso and racemic diastereomers in which the latter predominates, as is established by its separation and then reaction with optically pure (+)-2-methylbutyl iodide to give two diastereomeric products of Pt-Si bond cleavage as well as by single-crystal X-ray diffraction.

## Introduction

Some time ago we began to examine the usefulness of simultaneous silyl and phosphorus ligation as a methodology for modifying the molecular geometry of a transition-metal silyl complex to "anchor" the silicon center in the vicinity of a metal site.[2] This was conceived as a design for developing a configuration in which electron release from Si might exaggerate the electron-rich character of catalytically reactive platinum-group metal centers, and wherein nucleophilic substrate activation by the latter could cycle without concomitant capture and subsequent elimination of the silyl fragment in a classical "leaving group" sense. The objective was thus to retain the silyl group as an electronic influence within a complex coordination sphere by incorporating it into a polydentate ligand framework, the spatial demands of which might be separately tailored to contribute to catalytic selectivity or extended in an approach to catalyst immobilization. Hydrosilylation (i.e. Si-H bond oxidative addition) of low-valent metal complexes by the bifunctional silane $PPh_2CH_2CH_2SiMe_2H$ ("chelH") or related (phosphinoalkyl)silanes[3] has provided a general synthetic route to mono- and bischelate derivatives of the silyl $PPh_2CH_2CH_2SiMe_2$- (i.e. "chel"), in which a silicon-transition-element bond is supported by simultaneous phosphine coordination to the metal atom. The $(chel)_2$ assembly so obtained is represented by diastereoisomeric planar platinum(II) complexes,[2] enantiomeric 5- and 6-coordinate rhodium(III) and iridium(III) geometries,[4] and conformationally distinct dispositions around octahedral ruthenium(II) and osmium(II) centers.[5] While our primary concern has lain with elaboration toward more rigid polydentate (cage) coordination[1] and with catalysis,[6] formation of the $(chel)_2$ species focuses attention on two interesting considerations, viz (a) the relationship between the "chelate-assisted" addition step and precoordination through the donor (P) heteroatom and (b) the way in which approach of a second chel skeleton to the metal site is oriented by prior attachment of the first. These effects are discernible in chemistry that has led to the isolation[2] of $Pt(chel)_2$ and related molecules and has established conclusively that Pt(IV) species are indeed involved in the formation of these silyl-platinum(II) complexes, i.e., that a "chelate-assisted" addition is followed by elimination of HCl, although the mechanism of subsequent cleavage of Pt-Si bonds by this latter reagent remains uncertain. We have also used NMR spectroscopy to monitor the course of COD displacement from $[Pt(COD)Cl_2]$ (COD = cycloocta-1,5-diene), which is the most convenient synthetic route to the chelate ring structure in $[Pt(chel)_2]$; in this reaction, initial coordination through P can clearly be distinguished, confirming that the double Si-H bond addition at Pt does indeed constitute a "chelate-assisted" process. Existence[2] of the analogues $[Pt(PPh_2CH_2CH_2SiR^1R^2)_2]$ in an unequal diastereoisomer ratio that depends on the nature of $R^1$ vs $R^2$ further demonstrates the significance of ligand orientation effects around the reacting Pt center.

## Experimental Section

Synthetic manipulations were conducted under an atmosphere of dry dinitrogen gas, using standard vacuum/purge techniques. All solvents

(1) Part 9: Joslin, F. L.; Stobart, S. R. *J. Chem. Soc., Chem. Commun.* **1989**, 504.
(2) Holmes-Smith, R. D.; Stobart, S. R.; Cameron, T. S.; Jochem, K. *J. Chem. Soc., Chem. Commun.* **1981**, 937.
(3) Holmes-Smith, R. D.; Osei, R. D.; Stobart, S. R. *J. Chem. Soc., Perkin Trans. 1* **1983**, 861.
(4) Auburn, M. J.; Stobart, S. R. *Inorg. Chem.* **1985**, *24*, 318.
(5) Holmes-Smith, R. D.; Stobart, S. R.; Vefghi, R.; Zaworotko, M. J.; Jochem, K.; Cameron, T. S. *J. Chem. Soc., Dalton Trans.* **1987**, 969.
(6) Stobart, S. R.; Grundy, S. L.; Joslin, F. L. U.S. Patent 4, 950, 798 1990.

0020-1669/91/1330-3333$02.50/0 